

On the influence of anisotropy on the magnetic small-angle neutron scattering of superparamagnetic particles

A. Michels^a and J. Weissmüller

Institut für Nanotechnologie, Forschungszentrum Karlsruhe, Karlsruhe, Germany
Technische Physik, Universität des Saarlandes, Postfach 151150, Bau 43.2, 66041 Saarbrücken, Germany

Received 8 November 2001

Abstract. This paper presents a calculation of the magnetic small-angle neutron scattering cross-section resulting from a dilute ensemble of superparamagnetic particles exhibiting uniaxial magnetic anisotropy. We focus on the two experimentally relevant scattering geometries in which the incident neutron beam is perpendicular or parallel to an applied magnetic field, and we discuss several orientations of the anisotropy axes with respect to the field. Magnetic anisotropy has no influence on the magnetic small-angle neutron scattering when the particles are mobile, as is the case e.g. in ferrofluids, but, when the particles are embedded in a rigid non-magnetic matrix and the orientations of the anisotropy axes are fixed, significant deviations compared to the case of negligible anisotropy are expected. For the particular situation in which the anisotropy axes are parallel to the applied field, closed-form expressions suggest that an effective anisotropy energy or anisotropy-energy distribution can be determined from experimental scattering data.

PACS. 61.12.Ex Neutron scattering techniques (including small-angle scattering) – 75.30.Gw Magnetic anisotropy – 75.50.Tt Fine-particle systems; nanocrystalline materials

1 Introduction

Isolated single-domain particles of a ferromagnetic material become superparamagnetic when the temperature T is increased until it reaches the blocking temperature T_B , where the thermal energy $k_B T$ is comparable in magnitude to the energy barrier for magnetization reversal. Within the timescale of experiment, the magnetization will then adjust by thermal activation to the equilibrium value for the respective applied magnetic field and temperature; superparamagnetic systems are therefore non-hysteretic. A central parameter for the magnetic properties of such systems is the total anisotropy energy E_A , because it governs the field and temperature dependence of the magnetization isotherm. To a first approximation, the magnetization isotherms in the superparamagnetic regime are described by the Langevin function, which is independent of E_A , but the detailed field dependence of the magnetization does depend measurably on the magnitude of the anisotropy and on the orientation distribution of the easy axes. The magnitude of E_A can be estimated from the size and shape of the particles and data for the magnetocrystalline anisotropy of the coarse-grained material, but such estimates are often inaccurate, since they neglect the effects of lattice defects and the contribution of surface anisotropy, for which there are few reliable data. When the particle-size distribution in a sample is monodisperse, then E_A can

be determined by analysis of experimental magnetization isotherms or by measurement of the blocking temperature, which marks the transition between superparamagnetic behaviour and stable ferromagnetism. There have been many such studies, but important aspects of superparamagnetism remain the subject of active research, including the role of interparticle interactions and the relationship between the microstructure and the magnetic properties. A challenge for comparing model and experiment arises from the fact that in real materials the values of the relevant parameters of the microstructure – the particle size and the interparticle spacing – generally do not assume unique values; instead, these values are characterized by distributions of finite width that are not generally known to the desired accuracy.

The technique of small-angle neutron scattering (SANS) has contributed to the understanding of superparamagnetism, firstly because *magnetic* SANS provides information regarding the interparticle interactions and, secondly, because *nuclear* SANS allows the particle-size distribution to be quantified, and it provides at least qualitative information on the interparticle spacing. Among the topics investigated using SANS are e.g. the shape anisotropy of precipitates [1–3], the intraparticle structure (specifically, the possible existence of a non-magnetic, “dead” surface layer on the particles) [4–10], ferromagnetic correlations between particles [6,8,11–16], and the effect of a distribution of particle sizes on the magnetic SANS [17]. Moreover, inelastic neutron scattering and

^a e-mail: anmi@nano.uni-saarland.de

neutron spin-echo spectroscopy have provided evidence for the existence of a dual spin dynamics in superparamagnetic systems [18–21], namely longitudinal fluctuations of the magnetization vector among the easy axes of magnetization and collective magnetic oscillations of the spin system about an easy axis.

In all of the above-mentioned SANS studies, the influence of a magnetic anisotropy on the direction of a particle's magnetization vector \mathbf{M} is either not relevant or ignored, and the data analysis is based on the assumption that the magnetic energy of a particle depends only on the orientation of the magnetic moments relative to that of an external magnetic field, resulting in Langevin statistics. However, as is well known from magnetization studies (see, *e.g.*, Refs. [22–30]), the presence of a direction of easy magnetization, induced *e.g.* by the crystal structure, mechanical stress, the surface or by the shape of the particles, causes deviations from Langevin behaviour. Since magnetic neutron scattering depends on the orientation of \mathbf{M} through the Halpern-Johnson vector [31,32], it is straightforward to show that anisotropy also has an effect on the magnetic SANS cross-section of superparamagnetic particles – an influence that is expected to become more pronounced the smaller the particle size [33].

In this work, we explore the effect of magnetic anisotropy on the magnetic SANS, and we suggest that the analysis of magnetic-field dependent SANS data may provide an alternative method for measuring the anisotropy energy E_A such that E_A may be determined for individual size classes in a sample with a distribution of particle sizes. SANS may thereby supplement other methods commonly used to derive quantitative information on the anisotropy in a given sample, such as DC and AC-magnetization measurements, muon-spin relaxation, Mössbauer spectroscopy and inelastic neutron scattering [21].

2 The small-angle neutron scattering cross-section of a dilute assembly of superparamagnetic particles with anisotropy

In this section, we analyze the SANS of an array of superparamagnetic particles in a non-magnetic homogeneous matrix, and we explicitly account for the existence of a direction of easy magnetization within the particles. For such a sample, the macroscopic differential scattering cross-section $d\Sigma/d\Omega$ for elastic scattering at scattering vector \mathbf{q} , arising from an arrangement of N particles at positions \mathbf{x}_j , can be written as [31,32,34–36]

$$\frac{d\Sigma}{d\Omega}(\mathbf{q}) = \frac{1}{V} \left| \sum_{j=1}^N F_j(\mathbf{q}) \exp(i\mathbf{q} \cdot \mathbf{x}_j) \right|^2, \quad (1)$$

where V is the scattering volume, and $F_j(\mathbf{q})$ denotes the form factor of the j th particle. We assume that the particles and the matrix have uniform atomic density and composition, and that the particles have a magnetization

uniform in magnitude and direction; these assumptions exclude a possible difference between nuclear and magnetic particle form factors. If the scattering system is sufficiently dilute, interparticle interference effects can be neglected, and the SANS cross-sections of the individual particles are additive, so that equation (1) simplifies to

$$\begin{aligned} \frac{d\Sigma}{d\Omega}(\mathbf{q}) &= \frac{1}{V} \sum_{j=1}^N |F_j(\mathbf{q})|^2 \\ &= \frac{1}{V} \sum_{j=1}^N [(\Delta\delta_{\text{nuc}})^2 + \delta_{\text{mag}}^2 \sin^2 \alpha_j] h_j^2(\mathbf{q}). \end{aligned} \quad (2)$$

Here, the quantity $(\Delta\delta_{\text{nuc}})^2$ denotes the squared difference in the nuclear scattering-length densities between particle j and the non-magnetic matrix, δ_{mag}^2 is the magnetic scattering-length density contrast of the particle, α_j denotes the angle between the scattering vector \mathbf{q} and the particle magnetization vector \mathbf{M}_j [31,32], and $h_j^2(\mathbf{q}) = \left| \int_{V_{p,j}} \exp(i\mathbf{q} \cdot \mathbf{x}) d^3x \right|^2$. In equation (2), we have neglected the interference between the nuclear and the magnetic scattering amplitudes. If we further consider the scattering from N particles with identical size or, alternatively, scattering only by the particles of one size class, then equation (2) reduces to

$$\frac{d\Sigma}{d\Omega}(\mathbf{q}) = \frac{N}{V} [(\Delta\delta_{\text{nuc}})^2 + \delta_{\text{mag}}^2 \langle \sin^2 \alpha \rangle] h^2(\mathbf{q}), \quad (3)$$

where $\langle \sin^2 \alpha \rangle$ is the average over all particles in that size class.

The factor $\langle \sin^2 \alpha \rangle$ in equation (3) may vary as a function of an applied magnetic field \mathbf{H}_a . In an experiment in which only \mathbf{H}_a is changed, the variation of $\langle \sin^2 \alpha \rangle$ can be accurately measured. As we shall show below, $\langle \sin^2 \alpha \rangle$ depends on the anisotropy energy E_A , and it is therefore possible to obtain information regarding E_A from scattering data. The remainder of this article is mainly concerned with the computation of ensemble averages of $\langle \sin^2 \alpha \rangle$ for experimentally accessible scattering geometries.

For a general orientation of the unit scattering vector $\boldsymbol{\epsilon} = \mathbf{q}/q$ and of the unit magnetization vector $\mathbf{m} = \mathbf{M}/M_s$ of particle j , the function $\sin^2 \alpha$ can be expressed as [31,32]

$$\begin{aligned} \sin^2 \alpha &= 1 - (\boldsymbol{\epsilon} \cdot \mathbf{m})^2 \\ &= 1 - (\sin \vartheta \sin \gamma \cos(\xi - \beta) + \cos \vartheta \cos \gamma)^2, \end{aligned} \quad (4)$$

where $\boldsymbol{\epsilon} = (\sin \vartheta \cos \xi, \sin \vartheta \sin \xi, \cos \vartheta)$, $\mathbf{m} = (\sin \gamma \cos \beta, \sin \gamma \sin \beta, \cos \gamma)$ (compare Fig. 1), and M_s is the saturation magnetization of a particle with volume V_p . For conciseness, we have omitted the index j , and we will adhere to this in the following.

For the most common scattering geometries used in standard magnetic SANS experiments, equation (4) can be simplified. For example, consider a magnetic field \mathbf{H}_a applied to the sample in direction $\mathbf{e}_z = (0, 0, 1)$: (i) If we take the incoming neutron beam, characterized by its wavevector \mathbf{k}_0 , along $\mathbf{e}_x = (1, 0, 0)$, perpendicular

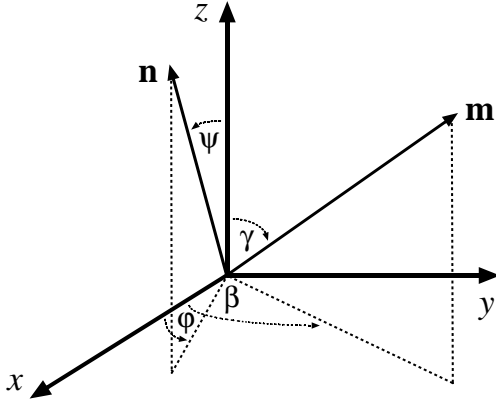


Fig. 1. The angles (γ, β) and (ψ, φ) define the respective orientations of the unit magnetization vector \mathbf{m} and the unit vector \mathbf{n} along the anisotropy axis.

to \mathbf{H}_a , then the scattering vector \mathbf{q} lies in the plane containing \mathbf{H}_a and $\mathbf{e}_y = (0, 1, 0)$; hence, $\xi = \pi/2$ and $\mathbf{q} = q(0, \sin \vartheta, \cos \vartheta)$. (ii) If we take \mathbf{k}_0 along \mathbf{e}_z , parallel to \mathbf{H}_a , then \mathbf{q} lies in the plane given by \mathbf{e}_x and \mathbf{e}_y ; thus, $\vartheta = \pi/2$ and $\mathbf{q} = q(\cos \xi, \sin \xi, 0)$. In the following, we refer to case (i) as the perpendicular scattering geometry and to case (ii) as the parallel geometry.

For the scattering geometries described above, the angles ϑ (case (i)) and ξ (case (ii)) specify the position of the scattering vector on the 2-dimensional detector, and radially averaging equation (4) leads to the following expressions:

$$\overline{\sin^2 \alpha} = \frac{1}{2\pi} \int_0^{2\pi} \sin^2 \alpha \, d\vartheta = 1 - \frac{1}{2} \sin^2 \gamma \sin^2 \beta - \frac{1}{2} \cos^2 \gamma \quad (5a)$$

for the perpendicular scattering geometry and

$$\overline{\sin^2 \alpha} = \frac{1}{2\pi} \int_0^{2\pi} \sin^2 \alpha \, d\xi = 1 - \frac{1}{2} \sin^2 \gamma \quad (5b)$$

for the parallel setup. We use the overline, $\overline{\sin^2 \alpha}$, to denote the average of the function $\sin^2 \alpha$ over the orientation of the scattering vector, and we use the bracket, $\langle \sin^2 \alpha \rangle$, to denote averaging over the orientation of the magnetization. Since SANS data obtained from isotropic microstructures are usually presented as a function of the modulus q of the scattering vector \mathbf{q} , we focus here on the computation of the radially-averaged scattering cross-section, which is independent of the orientation of \mathbf{q} . However, useful information can sometimes be obtained by analyzing the scattering measured along certain orientations on the 2-dimensional detector, as will be seen in Section 3.3 for the ratio of the SANS cross-sections with \mathbf{q} parallel and perpendicular to the applied magnetic field \mathbf{H}_a .

In order to calculate the magnetic-field dependent part of the SANS cross-section from a dilute dispersion of non-interacting superparamagnetic single-domain particles, we have to carry out averaging of equations (5a) and (5b). Of

interest here is the case when the particles are embedded in a solid non-magnetic matrix, so that the orientation $\mathbf{n} = (\sin \psi \cos \varphi, \sin \psi \sin \varphi, \cos \psi)$ of the anisotropy axis in each individual particle is fixed. The angular distribution of the anisotropy axes can then be described by the orientation distribution function $g(\psi, \varphi)$ [37] which is defined so that $\int_0^{4\pi} g(\psi, \varphi) \, d\Omega_n$ yields the total number N of particles within the scattering volume. For a fixed orientation (ψ, φ) of the anisotropy axis, one first has to thermally average the radially averaged expressions $\overline{\sin^2 \alpha(\mathbf{m})}$, equations (5a, 5b), with respect to all possible orientations of the reduced magnetization vector \mathbf{m} and then perform a statistical average over the weighting function $g(\psi, \varphi)$. In analogy to the well-known formalism developed *e.g.* in references [24–26] for the calculation of magnetization isotherms, the resulting expectation value $\langle \sin^2 \alpha \rangle$ for a monodisperse particle-size distribution is given by

$$\langle \sin^2 \alpha \rangle(h, k) = \frac{\int_0^{4\pi} \left[\frac{\int_0^{4\pi} \sin^2 \alpha \exp(-E/(k_B T)) \, d\Omega_m}{\int_0^{4\pi} \exp(-E/(k_B T)) \, d\Omega_m} \right] g(\psi, \varphi) \, d\Omega_n}{\int_0^{4\pi} g(\psi, \varphi) \, d\Omega_n} \quad (6)$$

The total magnetic energy of a single particle is denoted by E , k_B is the Boltzmann constant, T denotes the absolute temperature, and $d\Omega_m = \sin \gamma \, d\gamma \, d\beta$ and $d\Omega_n = \sin \psi \, d\psi \, d\varphi$ are the elements of solid angle in the direction of \mathbf{m} and in the direction of the anisotropy axis \mathbf{n} , respectively. See Figure 1 for an explanation of the angles involved in the calculations.

We write the total magnetic energy E of a single particle as the sum of a magnetic field energy $E_H = -\mu_0 V_p (\mathbf{M} \cdot \mathbf{H}_a)$ and of a contribution $E_A = -K_u V_p (\mathbf{m} \cdot \mathbf{n})^2$ due to a uniaxial magnetic anisotropy (compare Fig. 1),

$$E = E_H + E_A = -\mu_0 V_p M_s H_a \cos \gamma - K_u V_p (\sin \gamma \sin \psi \cos(\beta - \varphi) + \cos \gamma \cos \psi)^2, \quad (7)$$

where μ_0 is the permeability of free space, and $K_u > 0$ denotes a uniaxial anisotropy constant. Higher-order contributions to E_A are neglected, and we restrict our considerations to the case of a uniaxial anisotropy. A cubic anisotropy-energy symmetry can be treated analogously by considering the corresponding expansion for E_A (see, *e.g.*, Eq. (5.1.8) in Ref. [38]). The particular example of particles showing uniaxial anisotropy was merely chosen because of mathematical convenience and in order to demonstrate the effect. In experimental investigations of small magnetic particles, the physical origin of the anisotropy may have one or more sources, such as surface, shape or exchange effects, each of which can lead to a different anisotropy symmetry. Nevertheless, once that symmetry is known, its implementation in an expression for E is straightforward.

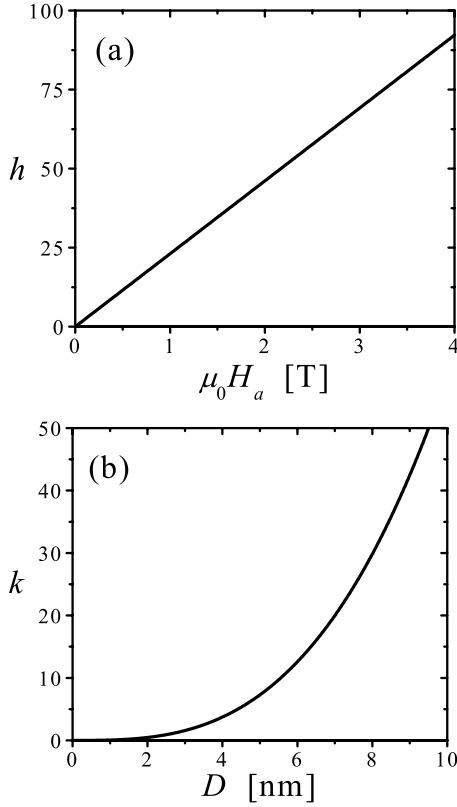


Fig. 2. (a) Magnetic-field parameter h plotted as a function of the applied magnetic field $\mu_0 H_a$; assumed particle diameter is $D = 5$ nm, $T = 295$ K and $M_s = 1434$ kA/m. (b) Anisotropy parameter k plotted as a function of particle size D , assuming $K_u = (4.53 \times 10^5)$ J/m³ and $T = 295$ K.

By insertion of equation (7) into equation (6), it is seen that the SANS cross-section depends on the magnitude of the applied magnetic field H_a through the magnetic-field parameter $h = \mu_0 V_p M_s H_a / (k_B T)$ and on the anisotropy constant K_u through the anisotropy parameter $k = K_u V_p / (k_B T)$. The typical range of experimental values of these parameters can be seen in Figure 2, where we plot h versus H_a for a spherical particle with a diameter $D = 5$ nm, assuming $M_s = 1434$ kA/m, as for bulk hcp-Co [39], and $T = 295$ K. Figure 2b depicts k as a function of D at $T = 295$ K using the single-crystal value $K_u = (4.53 \times 10^5)$ J/m³ for hcp-Co at $T = 288$ K [40]. Note that the value of k at the blocking temperature (of uniaxial particles) is about $k \approx 25$ [41], so that superparamagnetic behaviour is restricted to $k \lesssim 25$.

3 Results for the expectation value $\langle \sin^2 \alpha \rangle$

We have solved equation (6) numerically using Gauss-Legendre integration [42]. For some special orientations of the anisotropy axes, equation (6) can be integrated analytically (see Sect. 3.2.1). Likewise, in the case of zero anisotropy ($k = 0$), one obtains the following formulas by

evaluating equation (6) with $k = 0$:

$$\langle \sin^2 \alpha \rangle (h, k = 0) = \frac{1}{2} + \frac{L(h)}{2h} \quad (8a)$$

for the perpendicular geometry and

$$\langle \sin^2 \alpha \rangle (h, k = 0) = 1 - \frac{L(h)}{h} \quad (8b)$$

for the parallel geometry. $L(h) = (\coth h - 1/h)$ denotes the Langevin function. Since $L(h) \approx h/3$ for $h \ll 1$, equations (8a, 8b) both approach $2/3$ as $h \rightarrow 0$. As $h \rightarrow \infty$, equations (8a, 8b) have the limiting values of $1/2$ and 1 , respectively. Therefore, in the case of negligible anisotropy, the magnetic SANS of a dilute assembly of non-interacting superparamagnetic particles can change as a function of an applied magnetic field by 25% in the perpendicular scattering geometry and by 50% in the parallel geometry. In the following, we will label all calculated expectation values as $\langle \sin^2 \alpha \rangle$, and we refer to the text and the figure captions for the respective orientations of the incoming neutron beam, applied field and anisotropy axes.

3.1 Isotropic orientation of the anisotropy axes with respect to the applied magnetic field

The orientation distribution function for an isotropic distribution of the anisotropy axes is $g(\psi, \varphi) = N/(4\pi)$. The numerical solutions to equation (6) are plotted in Figures 3a and b as a function of the magnetic-field parameter h for several values of the anisotropy parameter k . As can be seen, the presence of a preferred direction within the particles has a strong effect in both scattering geometries on the expected magnetic SANS signal as compared to the case of zero anisotropy (dashed lines). To further illustrate this, in Figures 4a and b we plot the difference $\Delta \langle \sin^2 \alpha \rangle$ between the respective expectation values of Figures 3a and b with and without anisotropy, *i.e.* $\Delta \langle \sin^2 \alpha \rangle = |\langle \sin^2 \alpha \rangle (h, k) - \langle \sin^2 \alpha \rangle (h, 0)|$. When the incoming neutron beam is perpendicular to the applied field ($\mathbf{k}_0 \perp \mathbf{H}_a$, Fig. 3a), the expectation value $\langle \sin^2 \alpha \rangle$ decreases with increasing field h (for fixed k), approaching a limiting value of $1/2$. For a given value of h , the signal increases with increasing value of k , since the component of the magnetization \mathbf{M} perpendicular to the scattering vector \mathbf{q} becomes stronger, and by virtue of equation (4) the magnetic SANS increases. On the contrary, when $\mathbf{k}_0 \parallel \mathbf{H}_a$ (Fig. 3b), the magnetic scattering signal at a given k increases when h is increased, and, for fixed h , $\langle \sin^2 \alpha \rangle$ decreases when k is increased. In the parallel geometry, the scattering vector \mathbf{q} is always perpendicular to \mathbf{H}_a , and increasing the field leads to an increase of the component of \mathbf{M} that is perpendicular to \mathbf{q} . At a given h , an increased k corresponds to a stronger component of \mathbf{M} in the plane of \mathbf{q} ; hence, $\langle \sin^2 \alpha \rangle$ decreases in this situation. The $k = 0$ limiting values of $2/3$ as $h \rightarrow 0$ and $1/2$ or 1 as $h \rightarrow \infty$ are preserved in both geometries.

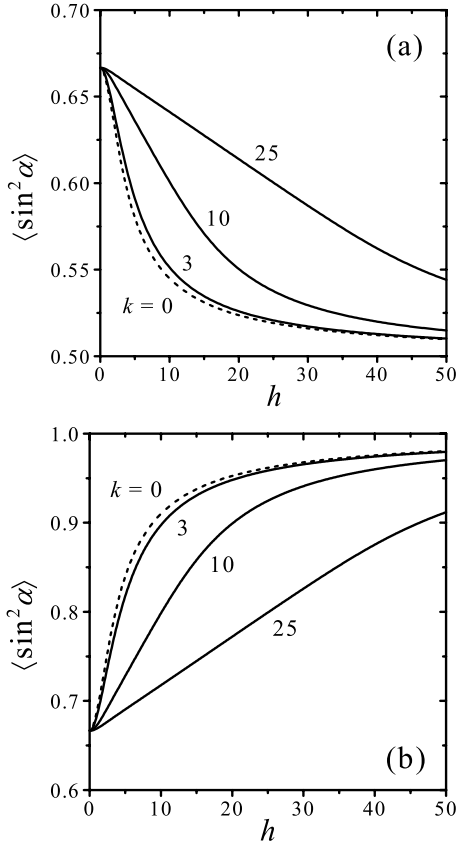


Fig. 3. Numerical solution to equation (6) for the general case of an isotropic distribution of uniaxial anisotropy axes. (a) Incoming neutron beam perpendicular to the applied magnetic field \mathbf{H}_a ($\mathbf{k}_0 \perp \mathbf{H}_a$). (b) $\mathbf{k}_0 \parallel \mathbf{H}_a$. Plotted is the respective expectation value as a function of the parameter h for k -values of 3, 10 and 25 (from bottom to top in (a) and from top to bottom in (b)). The dashed line in (a) and (b) refers, respectively, to the analytical solution for the case of zero anisotropy ($k = 0$), equations (8a, 8b).

In experimental studies, where anisotropy effects on the magnetic SANS are generally ignored, an applied magnetic field of the order of $\mu_0 H_a \cong 1$ T is often assumed to be sufficient to perfectly align the magnetic moments of all particles along \mathbf{H}_a . It is of interest to estimate the error involved in this assumption. For a fully saturated sample, $\langle \sin^2 \alpha \rangle \equiv 1/2$ in the perpendicular scattering geometry (compare Fig. 3a as $h \rightarrow \infty$). For spherical hcp-Co particles with a diameter $D = 6$ nm, $K_u = (4.53 \times 10^5)$ J/m³ and $M_s = 1434$ kA/m, a field $\mu_0 H_a = 1$ T corresponds to $h \approx 40$ at room temperature, and $k \approx 13$. The relative error in the magnetic SANS cross-section in the case of zero anisotropy, $[1 - 0.5/\langle \sin^2 \alpha \rangle(h = 40, k = 0)]$, amounts to about 2%. The presence of a non-negligible effective anisotropy ($k = 13$) increases the relative error to about 5%. However, in view of the (5 – 10)% error that is inevitably introduced by the SANS-data reduction procedure [43], this might be acceptable, at least for an isotropic distribution of anisotropy axes.

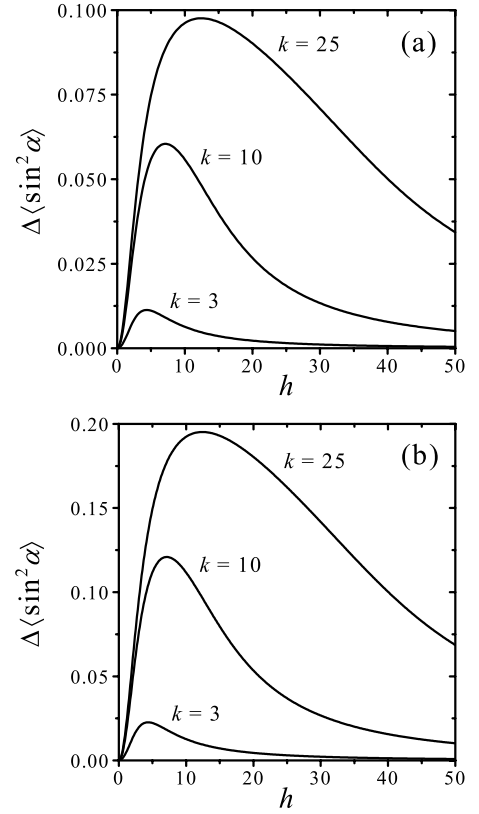


Fig. 4. Plot of the difference $\Delta \langle \sin^2 \alpha \rangle = |\langle \sin^2 \alpha \rangle(h, k) - \langle \sin^2 \alpha \rangle(h, 0)|$ as a function of h for different values of k (see inset) for the case of an isotropic distribution of anisotropy axes considered in Figure 3. (a) $\mathbf{k}_0 \perp \mathbf{H}_a$. (b) $\mathbf{k}_0 \parallel \mathbf{H}_a$.

If the magnetization vectors *and* the anisotropy axes of the individual particles are statistically distributed in *thermal equilibrium*, as is the case *e.g.* in a ferrofluid (fluid matrix), then the following equation has to be solved [24, 25]

$$\langle \sin^2 \alpha \rangle(h, k) = \frac{\int_0^{4\pi} \int_0^{4\pi} \sin^2 \alpha \exp(-E/(k_B T)) d\Omega_m d\Omega_n}{\int_0^{4\pi} \int_0^{4\pi} \exp(-E/(k_B T)) d\Omega_m d\Omega_n} . \quad (9)$$

As can be shown analytically using *e.g.* the procedure outlined in the Appendix of reference [24], the solutions to equation (9) for the two scattering geometries discussed above equal equations (8a, 8b), respectively, *i.e.* the presence of uniaxial anisotropy does not affect the magnetic SANS of particles that are allowed to move freely within the matrix. We have evaluated equation (9) numerically and confirmed that the results agree with equations (8a, 8b); this provides a check of our numerical procedure.

3.2 Special orientations of the anisotropy axes

The influence of uniaxial anisotropy becomes more significant when one considers fixed orientations (ψ^* , φ^*) of the anisotropy axes with respect to the direction of the external magnetic field. Then, $g(\psi, \varphi) d\Omega_n = N \delta(\psi - \psi^*) \delta(\varphi - \varphi^*) d\psi d\varphi$, with $\delta(x)$ denoting the delta function, and the total magnetic energy E of a single particle in equation (6) is evaluated at the particular values of ψ^* and φ^* . Such a preferred orientation (texture) of the anisotropy axes with respect to \mathbf{H}_a might be realized experimentally by freezing a ferrofluid in an applied magnetic field, by magnetic-field annealing of an amorphous precursor material during crystallization of the superparamagnetic particles, or by a mechanical treatment such as cold rolling. We will now discuss the solutions of equation (6) for the particular situations in which the anisotropy axes are oriented parallel or perpendicular to the applied field.

3.2.1 Anisotropy axes parallel to the applied magnetic field

For the case in which all anisotropy axes lie parallel to each other and parallel to the applied magnetic field \mathbf{H}_a , *i.e.* for $\psi^* = 0$, we can evaluate equation (6) analytically to obtain the following closed-form expressions:

$$\langle \sin^2 \alpha \rangle(h, k) = \frac{a \exp(b^2) - b \exp(a^2)}{\sqrt{16\pi k} [\operatorname{erfi}(b) - \operatorname{erfi}(a)]} - \frac{h^2 - 12k^2 - 2k}{16k^2} \quad (10a)$$

for the perpendicular scattering geometry and

$$\langle \sin^2 \alpha \rangle(h, k) = \frac{b \exp(a^2) - a \exp(b^2)}{\sqrt{4\pi k} [\operatorname{erfi}(b) - \operatorname{erfi}(a)]} + \frac{h^2 + 4k^2 - 2k}{8k^2} \quad (10b)$$

for the parallel scattering geometry, where $a = (h - 2k)/(2\sqrt{k})$, $b = (h + 2k)/(2\sqrt{k})$ and $\operatorname{erfi}(z) = 2/\sqrt{\pi} \int_0^z \exp(t^2) dt = -i \operatorname{erf}(iz)$ denotes the error function with complex argument. Equations (10a) and (10b) are plotted in Figures 5a and b, respectively.

3.2.2 Anisotropy axes perpendicular to the applied magnetic field

Figures 6a–d show the situation in which all anisotropy axes are parallel to each other and perpendicular to \mathbf{H}_a ($\psi^* = \pi/2$). In the perpendicular scattering geometry, the magnetic scattering depends on the orientation φ of the anisotropy axis \mathbf{n} in the plane perpendicular to \mathbf{H}_a . When the anisotropy axis is not contained in the plane formed by the scattering vector \mathbf{q} and \mathbf{H}_a then there is always a component of the magnetization perpendicular to \mathbf{q} . Hence, for a given value of h , this component (and hence the magnetic SANS) increases when the anisotropy parameter k is increased. In this geometry, we therefore expect the field dependence of the magnetic SANS to be

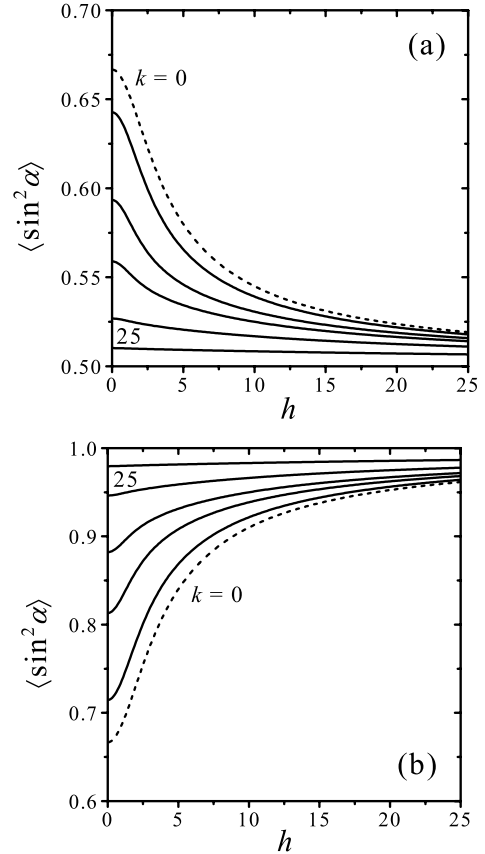


Fig. 5. The expectation value $\langle \sin^2 \alpha \rangle$ plotted as a function of h for several values of k for the case that all anisotropy axes are parallel to each other and parallel to the applied magnetic field \mathbf{H}_a ($\psi^* = 0$). (a) $\mathbf{k}_0 \perp \mathbf{H}_a$. (b) $\mathbf{k}_0 \parallel \mathbf{H}_a$. Solid curves: equations (10a, 10b), respectively, with $k = 1, 3, 5, 10, 25$ (from top to bottom in (a) and from bottom to top in (b)). Dashed lines: equations (8a, 8b), respectively.

largest when $\varphi^* = 0$ (or $\varphi^* = \pi$) and to be smallest when $\varphi^* = \pi/2$ (or $\varphi^* = 3\pi/2$). The solutions for the two extreme situations $\varphi^* = 0$ and $\varphi^* = \pi/2$ are shown in Figures 6a and b, respectively. In Figure 6c, we have plotted $\langle \sin^2 \alpha \rangle$ for the perpendicular geometry as a function of h for fixed $k = 3$ and for different values of the angle φ^* , illustrating the dependency of the magnetic SANS in this geometry on the orientation of the anisotropy axis in the plane perpendicular to \mathbf{H}_a . On the contrary, for $\mathbf{k}_0 \parallel \mathbf{H}_a$, all orientations φ^* are equivalent, and therefore all values of φ^* lead to the same $\langle \sin^2 \alpha \rangle$. Here, the presence of an anisotropy perpendicular to \mathbf{H}_a induces a component of \mathbf{M} parallel to \mathbf{q} ; hence, for a given h , $\langle \sin^2 \alpha \rangle$ decreases when k is increased.

In contrast to the general case of an isotropic distribution of the anisotropy axes (Fig. 3), the limiting values of $\langle \sin^2 \alpha \rangle$ for the special orientations $\psi^* = 0$ (Fig. 5) and $\psi^* = \pi/2$ (Fig. 6) take on different values from the anisotropy-free case ($k = 0$) as $h \rightarrow 0$. The magnetic SANS signal is now expected to change by about 50% (see, *e.g.*, Fig. 6a) as a function of the magnetic field h as compared to a change by 25% for the isotropic case in

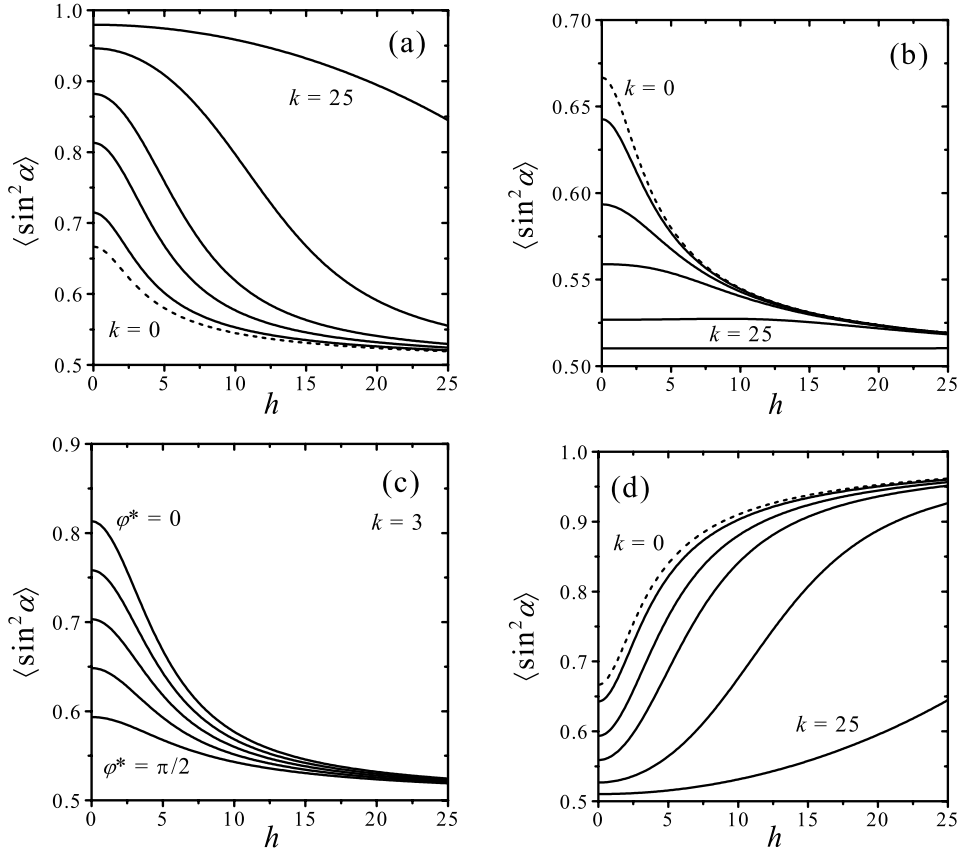


Fig. 6. The expectation value $\langle \sin^2 \alpha \rangle$ plotted as a function of h for several values of k for the case that all anisotropy axes are parallel to each other and perpendicular to the applied magnetic field \mathbf{H}_a ($\psi^* = \pi/2$). (a) $\mathbf{k}_0 \perp \mathbf{H}_a$ and $\varphi^* = 0$. (b) $\mathbf{k}_0 \perp \mathbf{H}_a$ and $\varphi^* = \pi/2$. (c) $\mathbf{k}_0 \perp \mathbf{H}_a$, $k = 3$ und $\varphi^* = 0, \pi/6, \pi/4, \pi/3, \pi/2$ (from top to bottom). (d) $\mathbf{k}_0 \parallel \mathbf{H}_a$ and φ^* arbitrary. Solid curves: $k = 1, 3, 5, 10, 25$ (from bottom to top in (a) and from top to bottom in (b) and (d)). Dashed line in (a), (b) and (d): equations (8a, 8b), respectively.

$$W(h, k) = \frac{(\Delta\delta_{\text{nuc}})^2 + \delta_{\text{mag}}^2 \left[\frac{a \exp(b^2) - b \exp(a^2)}{\sqrt{\pi} k [\text{erfi}(b) - \text{erfi}(a)]} - \frac{h^2 - 4k^2 - 2k}{4k^2} \right]}{(\Delta\delta_{\text{nuc}})^2 + \delta_{\text{mag}}^2 \left[\frac{b \exp(a^2) - a \exp(b^2)}{\sqrt{4\pi} k [\text{erfi}(b) - \text{erfi}(a)]} + \frac{h^2 + 4k^2 - 2k}{8k^2} \right]}. \quad (12)$$

the same scattering geometry (Fig. 3a). Therefore, large errors in the magnetic SANS may result when an asymptotical value of $2/3$ is assumed for $\langle \sin^2 \alpha \rangle$ at zero field for a textured sample.

3.3 Anisotropy of the scattering pattern

In addition to analyzing the total SANS cross-section $d\Sigma/d\Omega$ using the radially-averaged expectation value $\langle \sin^2 \alpha \rangle$, which is independent of the orientation of the scattering vector \mathbf{q} , one can also analyze the variation of $d\Sigma/d\Omega$ as a function of the angle between \mathbf{q} and the applied field \mathbf{H}_a . In some instances this might be more convenient or more accurate than the analysis of the field dependence of $d\Sigma/d\Omega$. In the following, we consider the ratio W of the total SANS cross-section $[d\Sigma/d\Omega]_{\mathbf{q} \parallel \mathbf{H}_a}$ with \mathbf{q} parallel to \mathbf{H}_a ($\vartheta = 0$ in Eq. (4)) to $[d\Sigma/d\Omega]_{\mathbf{q} \perp \mathbf{H}_a}$ with \mathbf{q}

perpendicular to \mathbf{H}_a ($\vartheta = \pi/2$ in Eq. (4)). For a monodisperse system of isotropic particles, W can be written as (compare Eq. (3))

$$W(h, k) = \frac{[d\Sigma/d\Omega]_{\mathbf{q} \parallel \mathbf{H}_a}}{[d\Sigma/d\Omega]_{\mathbf{q} \perp \mathbf{H}_a}} = \frac{(\Delta\delta_{\text{nuc}})^2 + \delta_{\text{mag}}^2 \langle \sin^2 \alpha \rangle_{\mathbf{q} \parallel \mathbf{H}_a}}{(\Delta\delta_{\text{nuc}})^2 + \delta_{\text{mag}}^2 \langle \sin^2 \alpha \rangle_{\mathbf{q} \perp \mathbf{H}_a}}. \quad (11)$$

Note that W is independent of q . In principle, all of the calculations for the perpendicular scattering geometry ($\mathbf{k}_0 \perp \mathbf{H}_a$) discussed in the previous sections can now be repeated in order to demonstrate the influence of a preferred direction within the particles on W . However, we focus here on the particular case of all anisotropy axes aligned parallel to \mathbf{H}_a ($\psi^* = 0$), for which the following closed-form solution exists:

(see equation (12) above.)

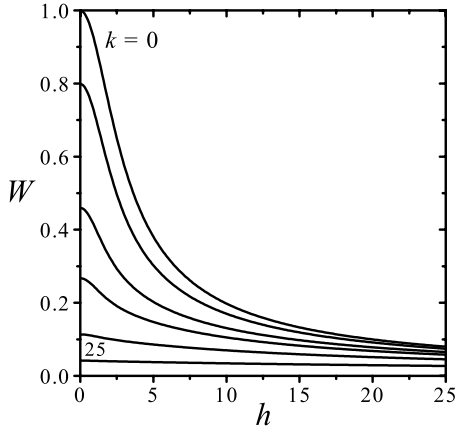


Fig. 7. Ratio W of the scattering cross-sections $[d\Sigma/d\Omega]_{\mathbf{q}\parallel\mathbf{H}_a}$ ($\vartheta = 0$) and $[d\Sigma/d\Omega]_{\mathbf{q}\perp\mathbf{H}_a}$ ($\vartheta = \pi/2$) (Eq. (12)) as a function of h in the perpendicular scattering geometry ($\mathbf{k}_0 \perp \mathbf{H}_a$). All anisotropy axes are assumed to be parallel to \mathbf{H}_a ($\psi^* = 0$), $(\Delta\delta_{\text{nuc}})^2 = 0$ and $k = 0, 1, 3, 5, 10, 25$ (from top to bottom).

Here, the parameters a and b and the function $\text{erfi}(z)$ have the same meaning as in equations (10). In Figure 7, we plot W from equation (12) as a function of the magnetic-field parameter h for several values of k , setting $(\Delta\delta_{\text{nuc}})^2 = 0$, *i.e.* we are considering purely magnetic scattering. A separation of nuclear and magnetic scattering contributions can be achieved in experiment through the application of a saturating magnetic field to the sample [44].

At zero field and for vanishing anisotropy, the magnetic scattering pattern on the detector is isotropic ($W = 1$), since the magnetization vectors of the individual particles take on all orientations with equal probability. For an increasing value of k and at a given h , the component m_z of the reduced magnetization \mathbf{m} (parallel to \mathbf{H}_a) increases, and, correspondingly, the components of \mathbf{m} which are perpendicular to \mathbf{H}_a decrease, so that $[d\Sigma/d\Omega]_{\mathbf{q}\parallel\mathbf{H}_a} \rightarrow 0$ and $[d\Sigma/d\Omega]_{\mathbf{q}\perp\mathbf{H}_a} \rightarrow 1$, leading to a decrease in W . For a sample with the corresponding texture ($\psi^* = 0$), a measurement of W at several applied fields may therefore yield information regarding the parameter k and, hence, the anisotropy energy E_A of the particles.

4 Influence of a distribution of particle sizes

All of the results presented in the previous sections have been obtained under the assumption that the sample consists of particles with a uniform size (and shape). However, as a consequence of the technique by which the sample is prepared, a certain degree of polydispersity is present in most cases, and, in general, the resulting distribution of anisotropy energies E_A will have an effect on the measured SANS signal. The total SANS cross-section at each discrete scattering vector q and applied magnetic field H_a is then given by the convolution of $d\Sigma/d\Omega$ for the monodisperse case with the particle-size distribution function $f(D)$, which is defined so that $f(D)dD$ equals the number of particles within the scattering volume with

diameters in the interval $[D, D+dD]$. The scattering cross-section is then (compare Eq. (3))

$$\frac{d\Sigma}{d\Omega}(q, H_a) = \frac{1}{V} \int_0^\infty [(\Delta\delta_{\text{nuc}})^2 + \delta_{\text{mag}}^2 \langle \sin^2 \alpha \rangle] h^2(q, D) f(D) dD, \quad (13)$$

where $\langle \sin^2 \alpha \rangle$ is a function of H_a and through the anisotropy energy E_A of the particle size D . Equation (13) can in principle be used in order to gain information about the size distribution of the anisotropy energies $E_A(D)$ in a given sample. For instance, by expanding $E_A(D)$ in a power series, $E_A = a_1 D^3 + a_2 D^2$, and assuming a particle shape and a lognormal particle-size distribution with 2 adjustable parameters, one can determine the parameter values a_1 and a_2 , which describe how E_A is distributed over the different size classes. Moreover, since the coefficients a_1 and a_2 reflect the contributions of volume and surface anisotropy, respectively, one may identify and quantify the dominating type of anisotropy in small magnetic particles. The fitting of experimental *magnetic* SANS data to equation (13) can be facilitated by the *independent* determination of the particle-size distribution $f(D)$ – for instance by *nuclear* SANS, small-angle X-ray scattering or transmission electron microscopy – with the result that the number of fit parameters in equation (13) is reduced.

5 Summary and conclusions

We have investigated the influence of uniaxial magnetic anisotropy on the magnetic SANS cross-section of a dilute array of superparamagnetic particles in a non-magnetic matrix. For the two most common SANS scattering geometries, in which the incident neutron beam is perpendicular or parallel to an applied magnetic field, and for several different orientations of the anisotropy axes with respect to the applied field, the field-dependent magnetic SANS was obtained by numerical integration of equation (6). If the particles are allowed to move freely within the matrix, then the presence of anisotropy does not influence the expectation value for $\langle \sin^2 \alpha \rangle$. However, when the particles are embedded in a solid non-magnetic environment, we find that a non-negligible anisotropy leads to significant deviations from the case of zero anisotropy. Therefore, special care should be taken in experiment to correct for anisotropy effects, in particular when assigning asymptotical values to $\langle \sin^2 \alpha \rangle$ in the cases of zero and large applied fields. For the particular situation of a texture parallel to the applied field, closed-form expressions could be derived for the radially-averaged SANS cross-section as well as for the ratio of cross-sections measured with the scattering vector along and perpendicular to the field. A comparison with experimental SANS data may in this case enable the magnitude and size distribution of the effective magnetic anisotropy energy E_A to be determined.

This work has been supported by the Deutsche Forschungsgemeinschaft (Sonderforschungsbereich 277). We thank C.E. Krill and R. Birringer for a critical reading of the manuscript.

References

1. M. Ernst, J. Schelten, W. Schmatz, *Phys. Status Solidi* **7**, 469 (1971).
2. G. Abersfelder, K. Noack, K. Stierstadt, J. Schelten, W. Schmatz, *Philos. Mag. B* **41**, 519 (1980).
3. P. Kournettas, K. Stierstadt, D. Schwahn, *Philos. Mag. B* **51**, 381 (1985).
4. M. Sato, K. Hirakawa, *J. Phys. Soc. Jpn* **39**, 1467 (1975).
5. D.J. Cebula, S.W. Charles, J. Popplewell, *Colloid Polym. Sci.* **259**, 395 (1981).
6. R. Pynn, J.B. Hayter, S.W. Charles, *Phys. Rev. Lett.* **51**, 710 (1983).
7. A.C. Nunes, C.F. Majkrzak, A.E. Berkowitz, *J. Magn. Magn. Mater.* **39**, 59 (1983).
8. S. Itoh, Y. Endoh, S.W. Charles, *J. Magn. Magn. Mater.* **111**, 56 (1992).
9. U. Lembke, A. Hoell, R. Kranold, R. Müller, W. Schüppel, G. Goerigk, R. Gilles, A. Wiedenmann, *J. Appl. Phys.* **85**, 2279 (1999).
10. A. Wiedenmann, *J. Appl. Cryst.* **33**, 428 (2000).
11. R. Cywinski, J.G. Booth, B.D. Rainford, *J. Phys. F* **7**, 2567 (1977).
12. R. Rosman, J.J.M. Janssen, M.Th. Rekveldt, *J. Appl. Phys.* **67**, 3072 (1990).
13. I. Mirebeau, C. Bellouard, M. Hennion, J.-L. Dormann, C. Djega-Mariadassou, M. Tessier, *J. Magn. Magn. Mater.* **104**, 1560 (1992).
14. J.R. Childress, C.L. Chien, J.J. Rhyne, R.W. Erwin, *J. Magn. Magn. Mater.* **104**, 1585 (1992).
15. C. Bellouard, I. Mirebeau, M. Hennion, *Phys. Rev. B* **53**, 5570 (1996).
16. J. Kohlbrecher, A. Wiedenmann, H. Wollenberger, *Z. Physik B* **104**, 1 (1997).
17. A.C. Nunes, *J. Appl. Cryst.* **21**, 129 (1988).
18. M. Hennion, C. Bellouard, I. Mirebeau, J.-L. Dormann, M. Nogues, *Europhys. Lett.* **25**, 43 (1994).
19. M.F. Hansen, F. Bødker, S. Mørup, K. Lefmann, K.N. Clausen, P.A. Lindgård, *Phys. Rev. Lett.* **79**, 4910 (1997).
20. H. Casalta, P. Schleger, C. Bellouard, M. Hennion, I. Mirebeau, G. Ehlers, B. Farago, J.-L. Dormann, M. Kelsch, M. Linde, F. Philipp, *Phys. Rev. Lett.* **82**, 1301 (1999).
21. M.F. Hansen, F. Bødker, S. Mørup, K. Lefmann, K.N. Clausen, P.-A. Lindgård, *J. Magn. Magn. Mater.* **221**, 10 (2000).
22. J.D. Livingston, C.P. Bean, *J. Appl. Phys.* **30**, 318S (1959).
23. F.G. West, *J. Appl. Phys.* **32**, 249S (1961).
24. I. Yasumori, D. Reinen, P.W. Selwood, *J. Appl. Phys.* **34**, 3544 (1963).
25. K. Müller, F. Thurley, *Int. J. Magn.* **5**, 203 (1973).
26. D.I. Paul, L.M. Pecora, *Phys. Rev. B* **19**, 4608 (1979).
27. Y.L. Raikher, *J. Magn. Magn. Mater.* **39**, 11 (1983).
28. R.W. Chantrell, N.Y. Ayoub, J. Popplewell, *J. Magn. Magn. Mater.* **53**, 199 (1985).
29. P.J. Gregg, L. Bessais, *J. Magn. Magn. Mater.* **202**, 554 (1999).
30. M. Respaud, *J. Appl. Phys.* **86**, 556 (1999).
31. O. Halpern, M.H. Johnson, *Phys. Rev.* **55**, 898 (1939).
32. G.E. Bacon, *Neutron Diffraction* (Clarendon Press, Oxford, 1955), Chap. VI.
33. F. Bødker, S. Mørup, S. Linderoth, *Phys. Rev. Lett.* **72**, 282 (1994).
34. A. Guinier, G. Fournet, *Small-angle Scattering of X-rays* (Wiley, New York, 1955), Chap. 2.
35. G. Porod, in *Small-angle X-ray Scattering*, edited by O. Glatter, O. Kratky (Academic Press, London, 1982), pp. 17–51.
36. S.-H. Chen, T.-L. Lin, in *Methods of Experimental Physics—Neutron Scattering*, edited by D.L. Price, K. Sköld (Academic Press, San Diego, 1987), Vol. 23-Part B, pp. 489–543.
37. J.E. Hilliard, *Trans. Met. Soc. AIME* **224**, 1201 (1962).
38. A. Aharoni, *Introduction to the Theory of Ferromagnetism* (Clarendon Press, Oxford, 1996).
39. K. Adachi, D. Bonnenberg, J.J.M. Franse, R. Gersdorf, K.A. Hempel, K. Kanematsu, S. Misawa, M. Shiga, M.B. Stearns, H.P.J. Wijn, in *Landolt-Börnstein Numerical Data and Functional Relationships in Science and Technology*, edited by H.P.J. Wijn (Springer-Verlag, Berlin, 1986), Vol. III/19a: *Magnetic Properties of Metals*, pp. 24–141.
40. S. Chikazumi, *Physics of Ferromagnetism* (Clarendon Press, Oxford, 1997), p. 249.
41. B.D. Cullity, *Introduction to Magnetic Materials* (Addison-Wesley Publishing Company, London, 1972), pp. 410–418.
42. J. Stoer, *Numerische Mathematik 1* (Springer-Verlag, Berlin, 1989), pp. 135–143.
43. C.J. Glinka, J.G. Barker, B. Hammouda, S. Krueger, J.J. Moyer, W.J. Orts, *J. Appl. Cryst.* **31**, 430 (1998).
44. C.G. Shull, E.O. Wollan, W.C. Koehler, *Phys. Rev.* **84**, 912 (1951).